

Real-Time Evaluation of Hydrogen Peroxide Injuries in Pulmonary Fibrosis Mice Models with a Mitochondria-Targeted Near-Infrared Fluorescent Probe

Xinyu Song,^{||} Song Bai,^{||} Na He, Rui Wang, Yanlong Xing,^{*} Changjun Lv,^{*} and Fabiao Yu^{*}



Cite This: *ACS Sens.* 2021, 6, 1228–1239



Read Online

ACCESS |



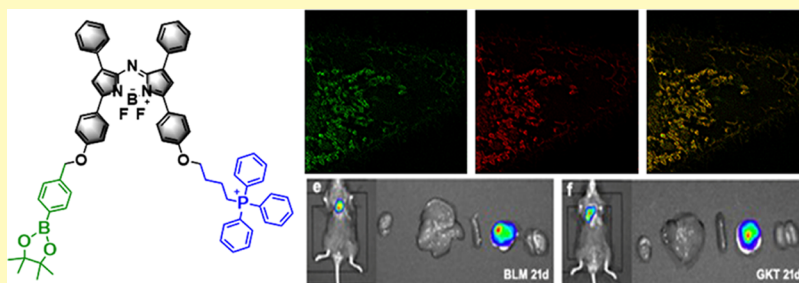
Metrics & More



Article Recommendations



Supporting Information



ABSTRACT: Pulmonary fibrosis is a fatal chronic lung disease, leading to poor prognosis and high mortality. Accumulating evidence suggests that oxidative stress characterized by excessive production of hydrogen peroxide (H_2O_2) is an important molecular mechanism causing pulmonary fibrosis. We conceive a new type of mitochondria-targeted near-infrared fluorescent probe Mito-Bor to investigate changes in the level of endogenous H_2O_2 in living cells and mice models with pulmonary fibrosis. In the design strategy of the Mito-Bor probe, we selected azo-BODIPY as the fluorophore owing to its near-infrared fluorescence, strong photochemical stability, and low biological toxicity. Under physiological conditions, the response moiety 4-bromomethylphenylboronic acid pinacol ester could easily detect H_2O_2 , and turn the fluorescence switch on. The modification of the lipophilic triphenylphosphine cation on the fluorophore would allow the probe to easily pass through the phospholipid bilayer of cells, and the internal positive charge could contribute to the selectivity of the mitochondria accumulation. The Mito-Bor probe provides high selectivity, low limit of detection, high biocompatibility, and excellent photostability. It can be used to detect changes in the level of H_2O_2 in living cells and in vivo. Therefore, the probe is applied to investigate the fluctuation of the H_2O_2 level during the process of inducing pulmonary fibrosis in cells, with changes in its fluorescence intensity correlating with the concentration of H_2O_2 and indicating the level of oxidative stress in fibroblasts. Conversely, pulmonary fibrosis can be modulated by adjusting the level of H_2O_2 in cells. A further study in mice models of bleomycin-induced pulmonary fibrosis confirms that NADPH oxidase 4 (NOX4) acts as a “button” to regulate H_2O_2 levels. The direct inhibition of NOX4 can significantly reduce the level of H_2O_2 , which can delay the progression of lung fibrosis. These results provide an innovative way for the clinical treatment of pulmonary fibrosis.

KEYWORDS: fluorescent probes, near-infrared, hydrogen peroxide, in vivo imaging, pulmonary fibrosis

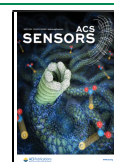
Pulmonary fibrosis, especially idiopathic pulmonary fibrosis (IPF), is a fatal chronic lung disease but with unknown etiological factors and pathogenesis that result in adverse prognosis.¹ The pathological changes caused by fibrosis is characterized by extracellular matrix deposition, and the patients suffer from progressive dyspnea from local to widespread fibrosis. Currently, the diagnosis of pulmonary fibrosis mainly depends on lung biopsy or computed tomography (CT). Although high-resolution CT can be utilized for accurate diagnosis of pulmonary fibrosis, the result of medical imaging just illustrates that the lesions have irreversibly formed and the symptom is hardly relieved. Despite the factors that contribute to the decrease of lung compliance, the exact mechanisms involved in the initiation, maintenance, and progression of pulmonary fibrosis are still

difficult to explicitly elaborate, which creates a challenge for the therapy of this disease. However, an increasing number of studies have confirmed that oxidative stress is a critical molecular factor in pulmonary fibrosis.^{2,3} Oxidative stress usually refers to the imbalance between reactive oxygen species (ROS) production and antioxidant defense,^{4–6} which will induce cell dysfunction and tissue damage.^{7,8} Compared to

Received: December 2, 2020

Accepted: January 20, 2021

Published: January 28, 2021



other organs, the lungs are particularly susceptible to oxidative stress. As one of the most representative members of ROS, hydrogen peroxide (H_2O_2) plays critical roles in physiological processes such as cell growth, proliferation, host defense, and immune response.^{9–11} However, aberrantly high levels of H_2O_2 will result in oxidative damage and thereby directly lead to the functional decline of cells.^{12,13} Given the signal/stress dichotomy roles of H_2O_2 , it is crucial to distinguish its beneficial effects from detrimental effects on pulmonary fibrosis.

The assays applied to living cells in vivo are often limited due to the dynamic changes of endogenous H_2O_2 , which promotes the exploitation of new chemical tools that can be employed for the real-time detection of changes in the level of intracellular H_2O_2 in situ.^{14,15} Among the reported chemical tools, activatable molecular fluorescence bioimaging is a powerful technique because of its noninvasive, biocompatible, and visualization features.^{16–21} Hitherto, different types of fluorescent probes have been developed for the specific detection of intracellular H_2O_2 in living systems. The response mechanism depends on the following main types of chemical strategies, (a) the hydroboration–oxidation reaction that converts an alkene into a neutral alcohol,^{22–27} (b) the Baeyer–Villiger oxidation rearrangement reaction,^{28–31} (c) the oxidation of phenol to quinone,^{32,33} (d) the tandem Payne/Dakin reaction,^{34,35} (e) the cleavage of arylsulfonylesters,^{36,37} (f) the metal-mediated redox reaction,³⁸ and the oxidation reaction of chalcogenides.^{39,40} Although many H_2O_2 fluorescent probes have been elaborately devised, most of them lack organelle-targeting capability and accumulate in the cytoplasm with free diffusion and random distribution. However, dynamic changes in H_2O_2 levels in the subcellular milieu is largely dependent on organelles, mainly mitochondria, which is considered to be the primary source of H_2O_2 due to their role in oxygen consumption in the cellular compartment. Mitochondria are the energy factory, which are engaged in a series of biological events including, calcium circulation, protein synthesis, and apoptosis pathways. Therefore, mitochondria-targeting fluorescent probes are required to investigate the fluctuations in H_2O_2 levels at the subcellular level. To develop an effective chemical tool for imaging H_2O_2 in living cells in vivo, an ideal fluorophore with near-infrared (NIR) wavelength ranging from 650 to 900 nm is desired.^{41–46} This is attributed to the biggest advantage of NIR absorption and emission in maximizing tissue penetration while avoiding the absorbance of heme in hemoglobin and myoglobin, water, and lipids.⁴⁷ To the best of our knowledge, there are merely a few fluorescent probes for examining changes in the level of H_2O_2 during the progression of pulmonary fibrosis, and thus, such fluorescent probes with superior performance are still urgently needed. In this work, we aim to construct a mitochondria-targeting NIR fluorescent probe with good biocompatibility, a distinct turn-on fluorescence switch, and specific selectivity for endogenous H_2O_2 detection in living cells and in mice models.

Herein, a NIR mitochondria-targeted fluorescent probe Mito-Bor was synthesized for the detection of H_2O_2 in living cell and mice models of pulmonary fibrosis. The Mito-Bor probe included three moieties: near-infrared fluorophore azo-BODIPY, H_2O_2 response group 4-(bromomethyl) phenylboronic acid pinacol ester, and the mitochondrial localization group triphenylphosphonium cation. The sensing mechanism was based on the response of aryl borate to H_2O_2 , then the

release of the fluorophore triggered the fluorescence emission. The probe had been successfully applied to detect changes in the level of endogenous H_2O_2 in different types of cells and mice models of pulmonary fibrosis. Our results demonstrated that the levels of intracellular H_2O_2 were closely associated with the progression of pulmonary fibrosis. The Mito-Bor probe not only provided a promising tool to reveal the role of H_2O_2 in the progression of pulmonary fibrosis but also indicated a potential approach for an auxiliary clinical diagnosis of IPF.

EXPERIMENTAL SECTION

Synthesis of the Mito-Bor Probe. The NIR fluorophore Mito-1 (423.2 mg, 0.5 mmol), 4-(bromomethyl) phenylborate pinacol ester (213.6 mg, 0.6 mmol), and Cs_2CO_3 (245 mg, 0.75 mmol) were mixed in N,N -dimethylformamide (15 mL) under Ar. The reaction was allowed to proceed at 80 °C for 8 h. After cooling to room temperature, the mixture was extracted with CH_2Cl_2 (100 mL) and H_2O (100 mL) three times. Then, the organic layer was retained and washed with saturated sodium bromide, and dried overnight with anhydrous sodium sulfate. Afterward, the dried organic layer was filtered off and removed by evaporating under reduced pressure to obtain the crude product, which was then purified by silica gel column chromatography ($\text{CH}_2\text{Cl}_2/\text{CH}_3\text{OH} = 99.8: 0.2$ v/v). The final product was obtained as a green solid. Yield: 278 mg, 52.3%. ^1H NMR (500 MHz, $\text{DMSO}-d_6$) δ (ppm): 8.34 (s, 1H), 8.22–8.16 (m, 5H), 8.08–8.06 (m, 2H), 7.95–7.71 (m, 16H), 7.68–7.43 (m, 7H), 7.39–7.32 (dd, 4H), 7.21–7.08 (dd, 2H), 6.52 (s, 1H), 5.76 (s, 1H), 5.17 (s, 2H), 4.21–4.20 (t, 2H), 3.72–3.67 (m, 2H), 1.99–1.95 (m, 2H), 1.77–1.74 (m, 2H), 1.29 (s, 12H). ^{13}C NMR (125 MHz, $\text{DMSO}-d_6$) δ (ppm): 163.69, 157.65, 153.59, 149.21, 154.87, 140.68, 138.78, 135.91, 135.82, 134.58, 133.14, 132.42, 131.38, 130.09, 128.36, 128.10, 127.15, 125.54, 123.83, 120.64, 116.43, 115.31, 115.06, 114.59, 99.33, 83.63, 83.39, 73.31, 69.89, 29.20, 24.83, 24.54. ES-MS: m/z $\text{C}_{67}\text{H}_{61}\text{B}_2\text{F}_2\text{N}_3\text{O}_4\text{P}^+$, calcd 1062.4548, $[\text{M}]^+$ 1062.4549.

Establishment of Pulmonary Fibrosis Cell Models. Human embryo lung fibroblast IMR-90 and MRC-5 cell lines were fused to ~80%. The cells were washed with PBS buffer, and 1 mL of trypsin was added for 1 min. After adding Dulbecco's Modified Eagle's Medium (containing 10% serum), the cell suspension was slowly pipetted and transferred to a centrifuge tube. After centrifugation at 1100 rpm/min for 5 min, the supernatant was discarded, and 2 mL of cell culture medium was added to adjust the cell numbers to $\sim 1.0 \times 10^6$ cells/mL. Then the cells were cultured in an incubator at 37 °C under 5% CO_2 for 24 h. The cell fibrosis models were stimulated by adding recombinant transforming growth factor $\beta 1$ (TGF- $\beta 1$) to a final concentration of 5 nM in serum-free medium for 24, 48, and 72 h, respectively. The cell models of the therapy groups were firstly stimulated with 5 nM TGF- $\beta 1$ for 72 h, then the culture medium was removed and replaced by serum-free medium containing 20 μM NOX4 inhibitor GKT137831, and then incubated for 48 h.

Establishment of Mice Models of Pulmonary Fibrosis. In our assays, 64 6-week-old C57BL/6 male mice were randomly assigned into 8 groups to establish the pulmonary fibrosis model. The control group a was given normal saline. The mice in other groups received a single intratracheal spray of bleomycin (5 mg/kg) to establish the murine pulmonary fibrosis model. After the intratracheal instillation of bleomycin for 7 days, all mice in the treatment groups were administrated with GKT137831 (60 mg/kg, twice a week) via gavage. Therefore, the mice were additionally divided into 7 days bleomycin group, 14 days bleomycin group, 14 days bleomycin + GKT137831 group, 21 days bleomycin group, 21 days bleomycin + GKT137831 group, 28 days bleomycin group, and 28 days bleomycin + GKT137831 group.

RESULTS AND DISCUSSION

Design Strategy of the Mito-Bor Probe. To obtain a mitochondria-targeting fluorescent probe for intracellular

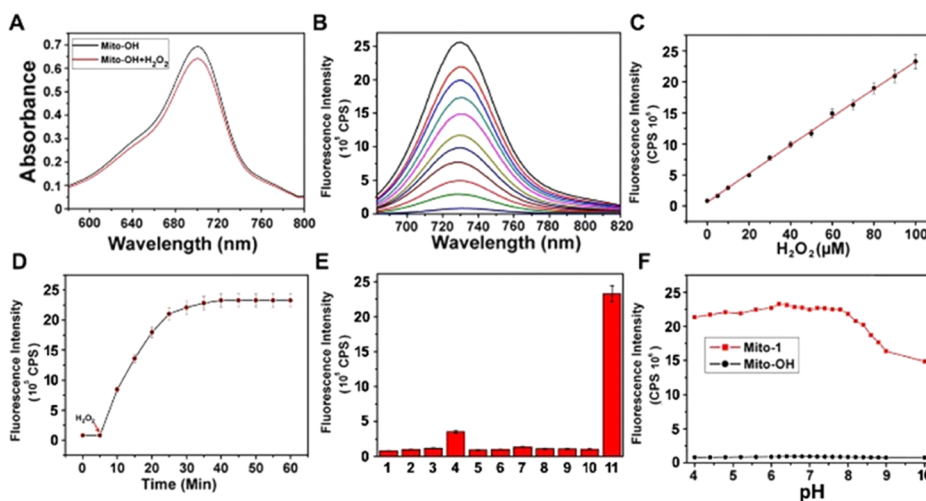
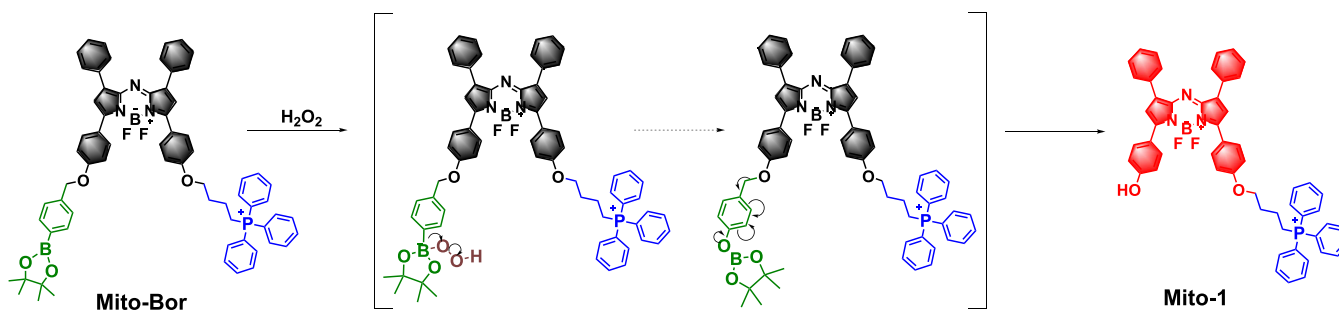
Scheme 1. Chemical Structure and Response Mechanism of the Mito-Bor Probe toward H₂O₂

Figure 1. Spectral properties of Mito-Bor. The concentration of the Mito-Bor probe used for analysis was 10 μM in 10 mM PBS buffer, pH 7.4. $\lambda_{\text{ex}} = 700 \text{ nm}$, $\lambda_{\text{em}} = 730 \text{ nm}$. (A) UV-vis spectra of Mito-Bor (black line) and reaction with 100 μM H₂O₂ (red line). (B) Changes in the fluorescence profile of Mito-Bor upon addition of H₂O₂ (0–100 μM). (C) Linear fitting equation between fluorescent intensities at 730 nm and H₂O₂ concentrations. (D) Reaction dynamics between Mito-Bor and 100 μM H₂O₂ during 0–60 min. (E) Selectivity toward biologically relevant reactive species. (1) Blank; (2) OCl⁻; (3) O₂⁻; (4) ONOO⁻; (5) NO; (6) methyl linoleate hydroperoxide (MeLOOH); (7) OH⁻; (8) glutathione (GSH); (9) vitamin C; (10) glucose; and (11) H₂O₂. All concentrations were 100 μM . (F) Fluorescence intensity changes in response to different pH values of the probe and reaction product, respectively. pH values: 4.0, 4.4, 4.8, 5.2, 5.6, 6.0, 6.2, 6.4, 6.6, 6.8, 7.0, 7.2, 7.4, 7.6, 7.8, 8.0, 8.2, 8.4, 8.6, 8.8, 9.0, and 10.0.

H₂O₂ detection, three essential challenges must be addressed (Scheme 1). The first step is the choice of the NIR fluorophore. As a typical BODIPY fluorophore, the azo-BODIPY dye exhibits NIR emission spectra, excellent photochemical stability, high molar absorption coefficients, low biological toxicity, and can be directly chemically modified.⁴⁸ Since the azo-BODIPY dye meets the common requirements for envisaging a probe, the off-on type of the probe remains desirable by taking advantage of the high sensitivity of a dark background. The second step is the selection of response moiety. As reported, the essential challenges for sensing H₂O₂ are chemoselectivity and biorthogonality.²² Therefore, in this work, we chose the H₂O₂-mediated boronate oxidation reaction-based strategy for H₂O₂ detection. Once masked with the 4-(bromomethyl)phenylboronic acid pinacol ester, the fluorescence of the azo-BODIPY fluorophore will be quenched because the boronate reaction site is a very strong Lewis acid, wherein the boron atom is sp²-hybridized with its vacant p-orbitals. We suppose that the fluorescence emission of the azo-BODIPY dye can be modulated via a photoinduced electron transfer (PET) process from the excited fluorophore to the response group (donor-excited PET, d-PET).³³ The last challenge is to determine the mitochondrial localization functional moiety. Fresh mitochondria

preserve their membrane at a unique negative potential of -180 mV . Fluorophores equipped with cationic ions are prone to cross the mitochondrial membranes and selectively target them. Therefore, the excellent hydrophobicity and strong negative potential accumulation make the triphenylphosphonium cation a suitable candidate for targeting mitochondria. Based on the abovementioned design strategies, we obtain the desired off-on fluorescent probe Mito-Bor for imaging of intracellular H₂O₂ (Scheme S1).

Spectral Properties and Sensing Behaviors of the Mito-Bor Probe. With the Mito-Bor probe in hand, we firstly evaluated its spectral properties and sensing behaviors toward H₂O₂ under simulated physiological conditions (10 mM PBS buffer, pH 7.4). As displayed in Figure 1A, the Mito-Bor probe (10 μM) exhibited a maximum absorption wavelength of 700 nm ($\epsilon_{700 \text{ nm}} = 6.8 \times 10^4 \text{ M}^{-1} \text{ cm}^{-1}$). The reaction with 100 μM H₂O₂ resulted in a slight decrease of the absorption band centered at 700 nm ($\epsilon_{700 \text{ nm}} = 6.2 \times 10^4 \text{ M}^{-1} \text{ cm}^{-1}$). As illustrated in Figure 1B, upon treatment with H₂O₂, the removal of response group 4-(bromomethyl)phenylboronic acid pinacol ester would hinder the d-PET process and release the azo-BODIPY fluorophore. The triggering of the off-on switch resulted in 25-fold fluorescence increase with emission centered at 730 nm using the excitation wavelength λ_{ex} at 700

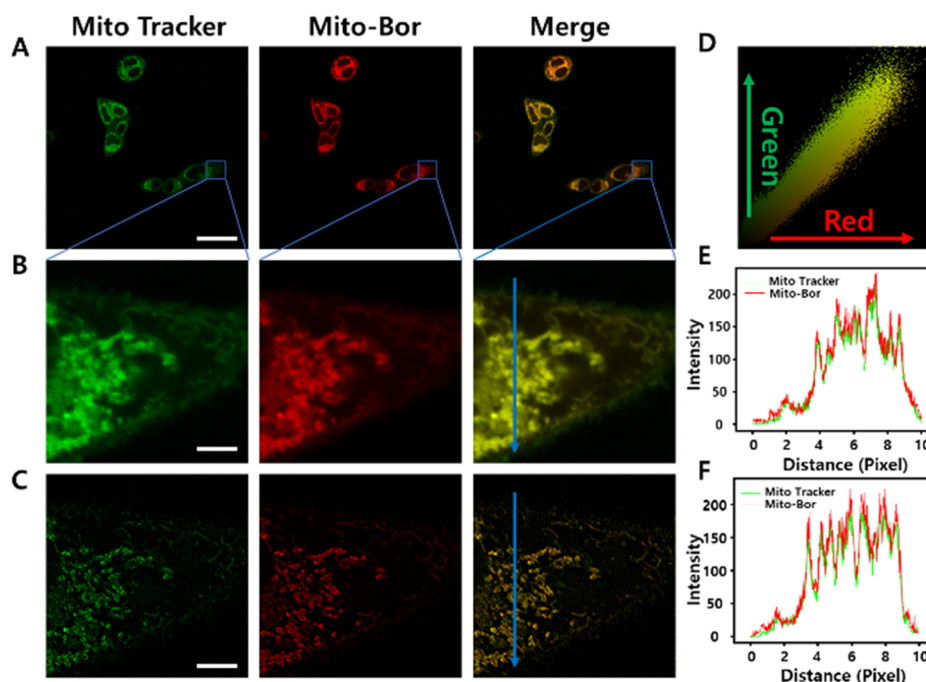


Figure 2. Determination of mitochondrial colocalization by super-resolution imaging of A549 cells. The cells were incubated with 10 μM Mito-Bor for 30 min and 1 $\mu\text{g}/\text{mL}$ MitoTracker Green FM dye for 15 min before imaging. The cells were washed three times with fresh cell culture medium. Fluorescence collection windows: green channel 500–550 nm ($\lambda_{\text{ex}} = 488$ nm) and red channel 700–800 nm ($\lambda_{\text{ex}} = 633$ nm). (A) Cells stained with MitoTracker Green FM and Mito-Bor. Scale bar: 10 μm . (B) Region of Interest in the blue frame of (A). (C) Image analysis by super-resolution imaging of mitochondria in (B), scale bar: 2 μm . (D) Correlation plot of the dyads in the merged region between green and red channels in (A). (E, F) Intensity profiles along the blue arrows in (B) and (C) across the cell, respectively.

nm. The quantum yield of our probe increased from 0.007 to 0.40 with a 57-fold enhancement. The fluorescence intensity increased following the increase of the H_2O_2 concentration (0–100 μM). The linear relationship between the fluorescence intensities and H_2O_2 concentrations was assessed via regression analysis. The regression equation was $F_{730\text{nm}} = 24\,423 [\text{H}_2\text{O}_2] (\mu\text{M}) + 17\,809$ with a good linear fitting constant $r = 0.9988$ (Figure 1C). The limit of detection (LOD) was determined to be less than 0.1 μM under our experimental conditions, and the theoretical estimation based on the linear calibration ($3\sigma/k$) proposed the LOD as low as 23 nM. The reaction dynamics was next examined with 10 μM Mito-Bor toward 100 μM H_2O_2 under simulated physiological conditions (Figure 1D). Upon adding H_2O_2 , the fluorescence response of Mito-Bor increased immediately and reached the plateau within 25 min. The selectivity of the probe toward H_2O_2 against ROS, reactive nitrogen species (RNS), and other biologically relevant reactive species was tested. The results indicated that our probe was extremely specific toward H_2O_2 , while other potential interfering species hardly induced any fluorescence responses (Figure 1E). Notably, even 100 μM peroxynitrite (ONOO^-) resulted in a slight fluorescence increase, indicating the negligible interference from the low physiological level of ONOO^- .⁴⁹ Moreover, other tested bio-species such as glutathione (GSH), vitamin C, and glucose-induced no change in the fluorescence signal. These results suggested the selective sensing capability of the Mito-Bor probe toward H_2O_2 . Additionally, the pH effects on fluorescence changes were recorded with pH values ranging from 4.0 to 10.0. As demonstrated in Figure 1F, the fluorescence intensities provided no distinct pH-dependence under the physiological conditions from pH 7.20 to pH 7.45. All of these results clearly illustrated that the Mito-Bor probe

could be utilized to selectively and sensitively examine changes in the level of H_2O_2 in the complicated physiological milieu.

Cytotoxicity and Evaluation of Mitochondrial Colocalization by Super-Resolution Imaging. We next employed Mito-Bor to investigate changes in endogenous H_2O_2 levels in living cells. A higher oxidative stress level has been observed in a variety of cancer cells compared to normal cells, mainly due to the excessive accumulation of ROS, especially the relatively stable H_2O_2 . To verify the universality of our probe for intracellular H_2O_2 detection, two kinds of human-derived non-small cell lung cancer cell lines (A549 cells and PC9 cells) were selected as the testing models. Prior to imaging, cytotoxicity assays of the Mito-Bor probe were performed with Cell Counting Kit-8 (CCK8) after incubating the cells with a serial concentration of Mito-Bor (0–100 μM) for 24 h. The results demonstrated that the Mito-Bor probe showed negligible cytotoxicity and could be utilized for imaging of intracellular H_2O_2 (Figure S1).

As mitochondria are the major source of H_2O_2 , the mitochondria-targeting capability of Mito-Bor is vital for detecting changes in the level of H_2O_2 . Next, we evaluated the mitochondrial localization performance of the Mito-Bor probe through a mitochondrial colocalization assay using A549 cells. A commercial mitochondrial dye (MitoTracker Green FM dye) was selected to co-incubate with the Mito-Bor probe. After incubating the cells with Mito-Bor for 30 min and MitoTracker Green FM dye for 15 min, they were washed three times with the fresh cell culture medium before imaging. As illustrated in Figure 2A, the fluorescence of the MitoTracker Green FM dye was observed in the green channel, and the Mito-Bor probe emitted its fluorescence in the red channel. The color pairs of each pixel of both channels implied a high correlated plot (Figure 2D). The correlation

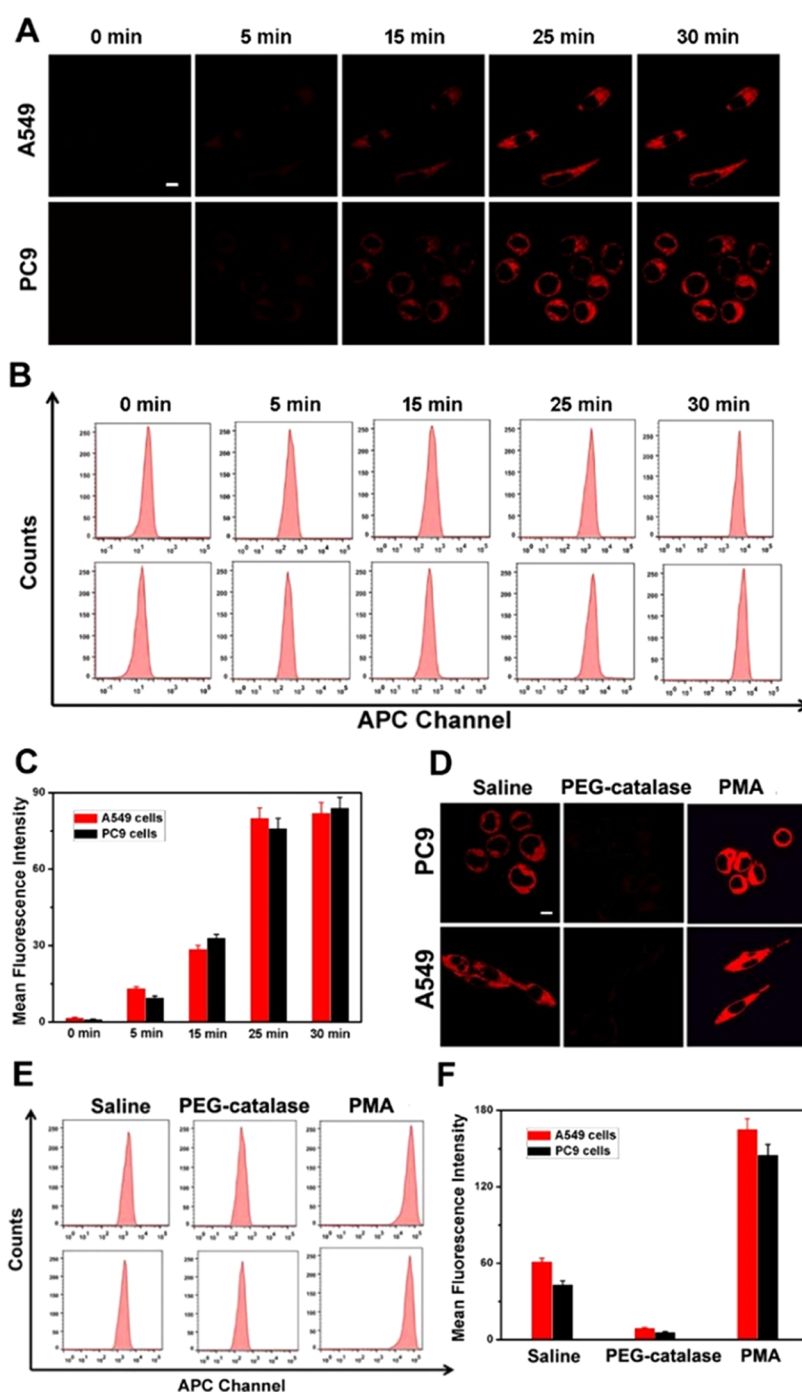


Figure 3. Evaluation of the endogenous H_2O_2 in A549 and PC9 lung cancer cells. The cells were treated with $10 \mu\text{M}$ Mito-OH for 30 min at 37°C before imaging. All images were imaged using a confocal laser scanning microscope (objective lens $\times 60$) with the collection fluorescence windows of $700\text{--}800 \text{ nm}$ ($\lambda_{\text{ex}} = 635 \text{ nm}$). The fluorescence channel of flow cytometry was collected by the APC channel. (A) Time-dependent fluorescence images of the A549 cells and PC9 cells. Scale bars: $10 \mu\text{m}$. (B) Flow cytometry analysis of A549 cells and PC9 cells, as in (A). (C) Histogram of the results shown in (B). (D) Fluorescence images of A549 cells and PC9 cells cultured with saline, cell-permeable catalase-poly(ethylene glycol) (PEG-catalase, 500 U/mL), and phorbol myristate acetate (PMA, $2 \mu\text{g/mL}$), respectively. Scale bars: $10 \mu\text{m}$. (E) Flow cytometry analysis of A549 cells and PC9 cells used in (D). (F) Histogram of the results shown in (E).

analysis suggested the Pearson's coefficient was $R_r = 0.98$, and the Manders' coefficients were $m_1 = 0.99$ and $m_2 = 0.98$. We also verified the applicability of Mito-Bor in mitochondrial localization via the super-resolution imaging technology. The images shown in Figure 2B were obtained by laser scanning confocal microscopy, while those displayed in Figure 2C were super-resolution images that evidently indicated the mitochondrial localization. Therefore, Mito-Bor could selectively

accumulate in the mitochondria rather than other organelles. The intensity profiles along the blue arrows in A549 cells were perfectly synchronous, while the super-resolution images revealed a more closely accurate plot (Figure 3E,F). All of these results demonstrated that the Mito-Bor probe could specifically localize in the mitochondria.

Evaluation of Endogenous H_2O_2 in Lung Cancer Cells. The rapid fluorescence response, low LOD, outstanding

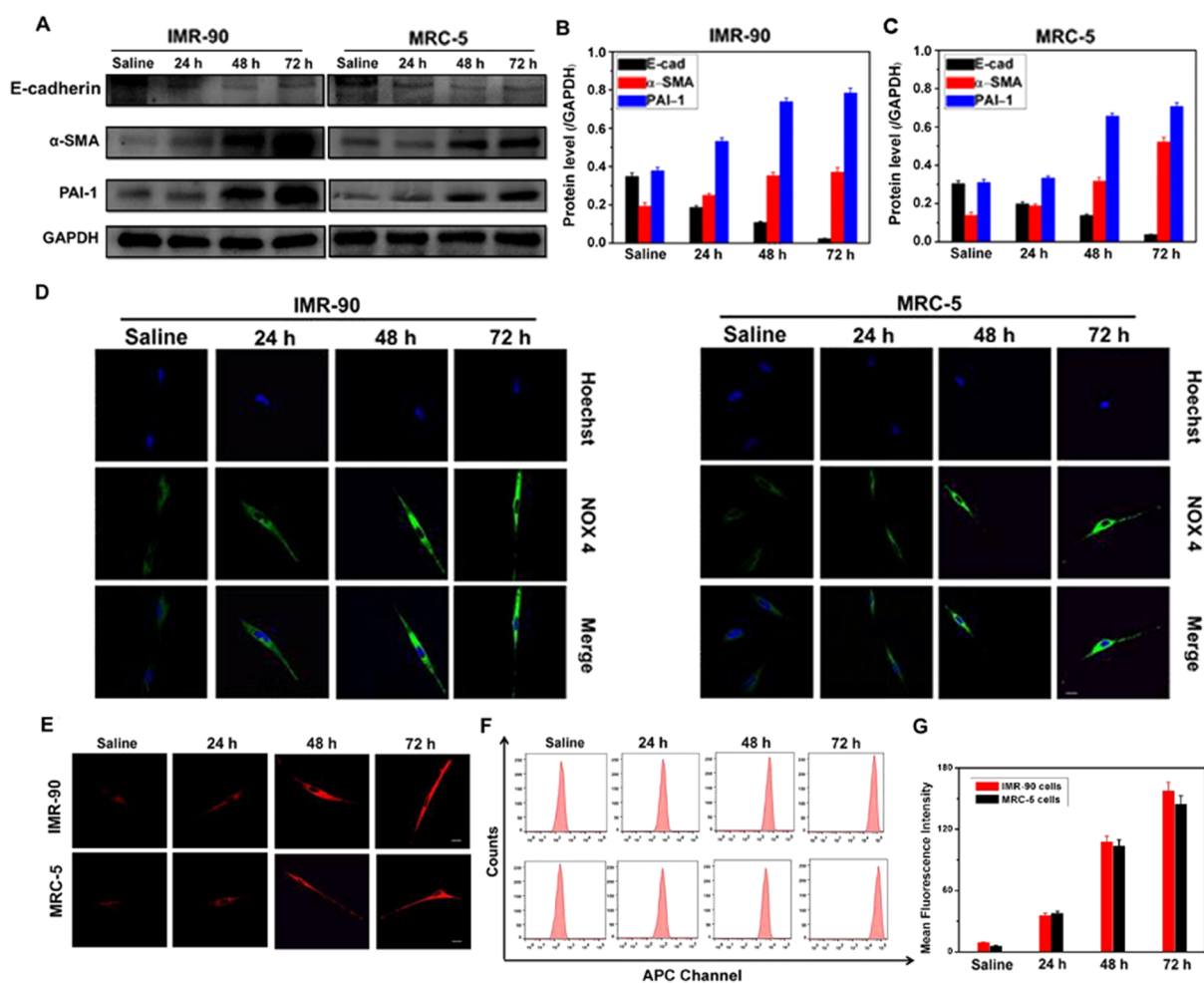


Figure 4. Investigation of changes in the H_2O_2 level in pulmonary fibrosis cell models. IMR-90 cells and MRC-5 cells were treated with serum-free media containing TGF- β 1 (5 nM) for 24, 48, and 72 h, respectively. (A) Western blot analysis of E-cadherin, α -SMA, and PAI-1 in IMR-90 cells and MRC-5 cells. GAPDH was used as the loading control. (B) and (C) Quantized histogram for the expression of E-cadherin, α -SMA, and PAI-1 in IMR-90 cells and MRC-5 cells. (D) NOX4 immunofluorescence images. IMR-90 cells and MRC-5 cells were incubated with recombinant anti-NADPH oxidase 4 antibody (1:100, Alexa Fluor 488) in the collection wavelength range of 500–550 nm ($\lambda_{\text{ex}} = 488$ nm). Nuclei were stained with Hoechst 33342 0.5 $\mu\text{g}/\text{mL}$ for 20 min in the collection wavelength range of 420–480 nm ($\lambda_{\text{ex}} = 405$ nm). Scale bars: 20 μm . (E) Imaging of changes in the H_2O_2 level in IMR-90 cells and MRC-5 cells. $\lambda_{\text{ex}} = 635$ nm. Fluorescence collection window: 700–800 nm. The cells were pretreated with TGF- β 1, and then incubated with Mito-Bor (10 μM) for 30 min at 37 $^\circ\text{C}$ before imaging. Scale bars: 20 μm . (F) Flow cytometry analysis of the cells in (E). (G) Histogram of the fluorescence intensities in (F).

selectivity, and low cytotoxicity of the Mito-Bor probe implied that it could be employed as a powerful chemical tool to investigate H_2O_2 related pathological processes. As illustrated in Figure 3A, the A549 and PC9 cell lines were both incubated with 10 μM Mito-Bor at 37 $^\circ\text{C}$ for 30 min before imaging. Both types of cell lines exhibited NIR fluorescence after 5 min of incubation. The fluorescence intensities increased with time and reached the plateau at 25 min. Extended incubation for 30 min did not induce a significant fluorescence increase. The flow cytometry results in Figure 3B,C were consistent with the fluorescence changes illustrated in Figure 3A. These results suggested that the Mito-Bor probe could detect the endogenous H_2O_2 concentration of A549 and PC9 cells within 25 min. To further verify the applicability of our probe, the two cell lines were treated with the cell-permeable catalase-poly(ethylene glycol) (PEG-catalase), which could scavenge the intracellular H_2O_2 , and phorbol myristate acetate (PMA), which could inhibit the mitochondrial respiratory chain and lead to a burst of H_2O_2 . Both cell groups were pretreated with 500 U/mL PEG-catalase and 2 $\mu\text{g}/\text{mL}$ PMA for 3 h as the

negative and positive control, respectively. After washing with fresh cell culture medium, the cells were incubated with the Mito-Bor probe (10 μM) for 30 min before imaging. As illustrated in Figure 3D, the A549 and PC9 cells in the PEG-catalase-treated group exhibited negligible fluorescence compared with the cells in the control group. However, in the PMA-treated group, much stronger fluorescence was detected. In addition, the flow cytometry analysis in Figure 3E,F provided consistent results with fluorescence changes in Figure 3D. These results demonstrated that our probe Mito-Bor could respond to changes in intracellular levels of H_2O_2 .

Investigation of Changes in H_2O_2 Levels in Pulmonary Fibrosis Cell Models. Oxidative stress caused by excessive ROS greatly influences the progression of pulmonary fibrosis. It was considered that H_2O_2 was one of the major ROS which could aggravate the degree of pulmonary fibrosis.^{50–52} Thus, we next applied the Mito-Bor to examine the level of fluctuation of H_2O_2 level in pulmonary fibrosis cell models. The epithelial–mesenchymal transdifferentiation (EMT) was a common molecular biological change observed

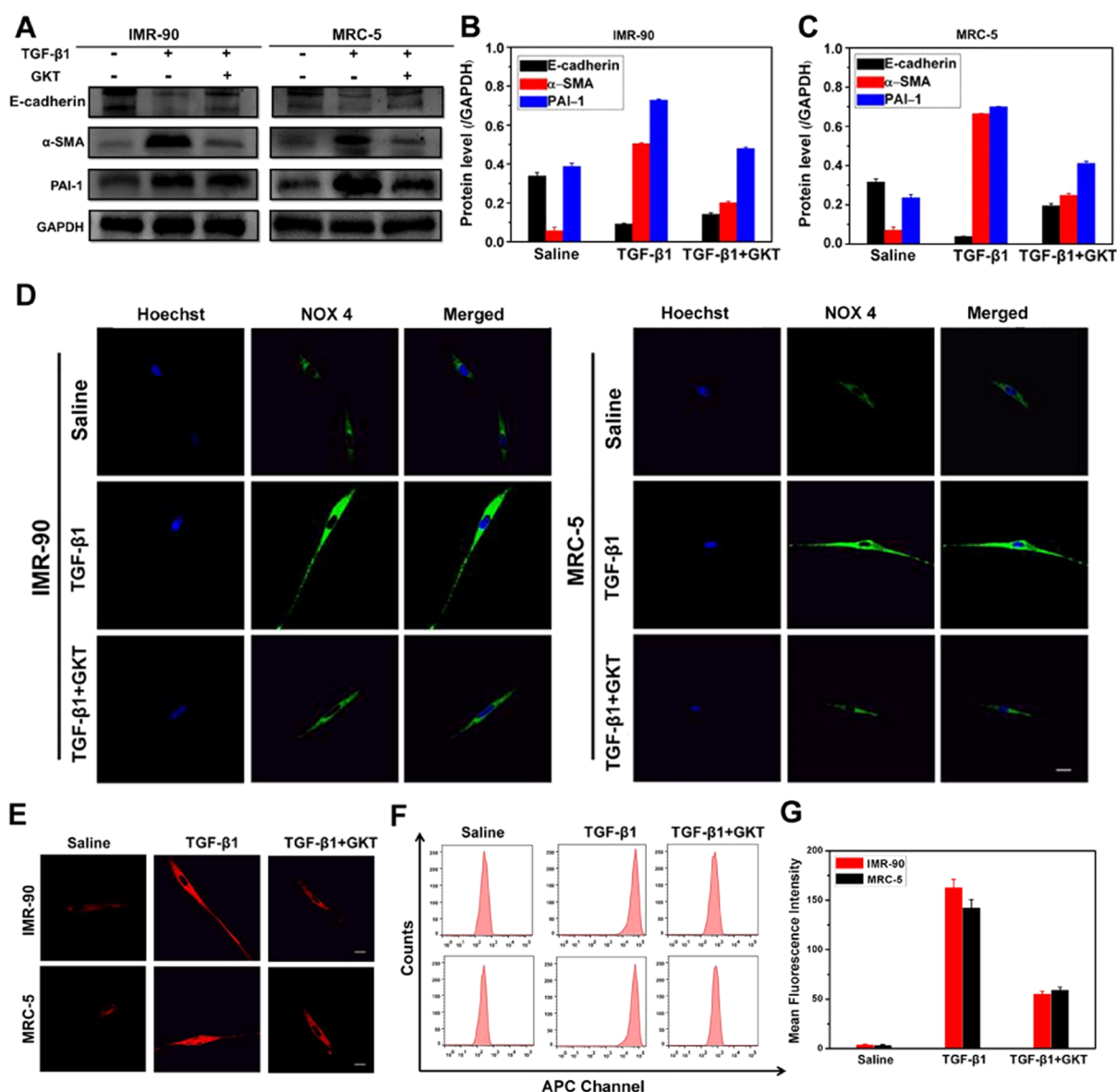


Figure 5. Evaluation of endogenous H_2O_2 levels during fibrosis progression. All IMR-90 cells and MRC-5 cells were cultured in serum-free medium as control. To construct cell models, the cell lines were treated with TGF- β 1 (5 nM) for 72 h at 37°C. A third group was further washed and incubated with a specific NOX4 inhibitor GKT (20 μM) at 37°C for 48 h. (A) Western blot analysis of the E-cadherin, α -SMA, and PAI-1 expression levels in IMR-90 and MRC-5 cells, respectively. GAPDH was used as the loading control. (B) and (C) are the histograms of the E-cadherin, α -SMA, and PAI-1 expression of IMR-90 cells and MRC-5 cells. (D) NOX4 immunofluorescence imaging of IMR-90 cells and MRC-5 cells with recombinant anti-NADPH oxidase 4 antibody (1:100, Alexa Fluor 488), the collection wavelength range was 500–550 nm ($\lambda_{\text{ex}} = 488$ nm). Nuclei were stained with 0.5 $\mu\text{g}/\text{mL}$ Hoechst 33342 for 20 min with the collection wavelength range of 420–480 nm ($\lambda_{\text{ex}} = 405$ nm). Scale bars: 20 μm . (E) Fluorescence Imaging of H_2O_2 levels in IMR-90 cells and MRC-5 cells. The cells were treated with Mito-Bor (10 μM) for 30 min at 37°C before testing. The image collection wavelength range was 700–800 nm ($\lambda_{\text{ex}} = 635$ nm). (F) Flow cytometry analysis of IMR-90 cells and MRC-5 cells in (E). (G) Histogram of the results in figure (F).

during fibrosis progression, which transformed healthy fibroblasts into myofibroblasts. During the development of EMT, the epithelial related expression reduced, while the mesenchymal related expression increased. As a ubiquitous profibrotic cytokine, transforming growth factor β (TGF- β) played critical roles in the progression of fibrosis. Furthermore, we took TGF- β 1 (a subtypes of TGF- β) as an EMT stimulus to induce fibrosis. Herein, human embryonic fibroblast IMR-90 cells and MRC-5 cells were treated with 5 nM TGF- β 1 for 24, 48, and 72 h, respectively. Changes in the epithelial marker (E-cadherin), mesenchymal marker (α -SMA), and plasminogen activator inhibitor-1 (PAI-1) were examined by western

blot analysis. As displayed in Figure 4A–C, both cell lines exhibited similar trends in the protein expression, with the downregulation of E-cadherin and the upregulation of α -SMA. PAI-1, a serine protease that inhibited fibrinolysis and extracellular matrix degradation, was involved in fibrosis in rats. The treatment with TGF- β led to a higher level of PAI-1 than that of the control group. The above results indicated that the fibrosis induced by TGF- β 1 showed a gradual progression trend. During this process, the epithelial cells gradually lost their characteristics but acquired those of mesenchymal cells. As the extracellular matrix increased, the degree of fibrosis became serious. NOX4 was involved in myofibroblast

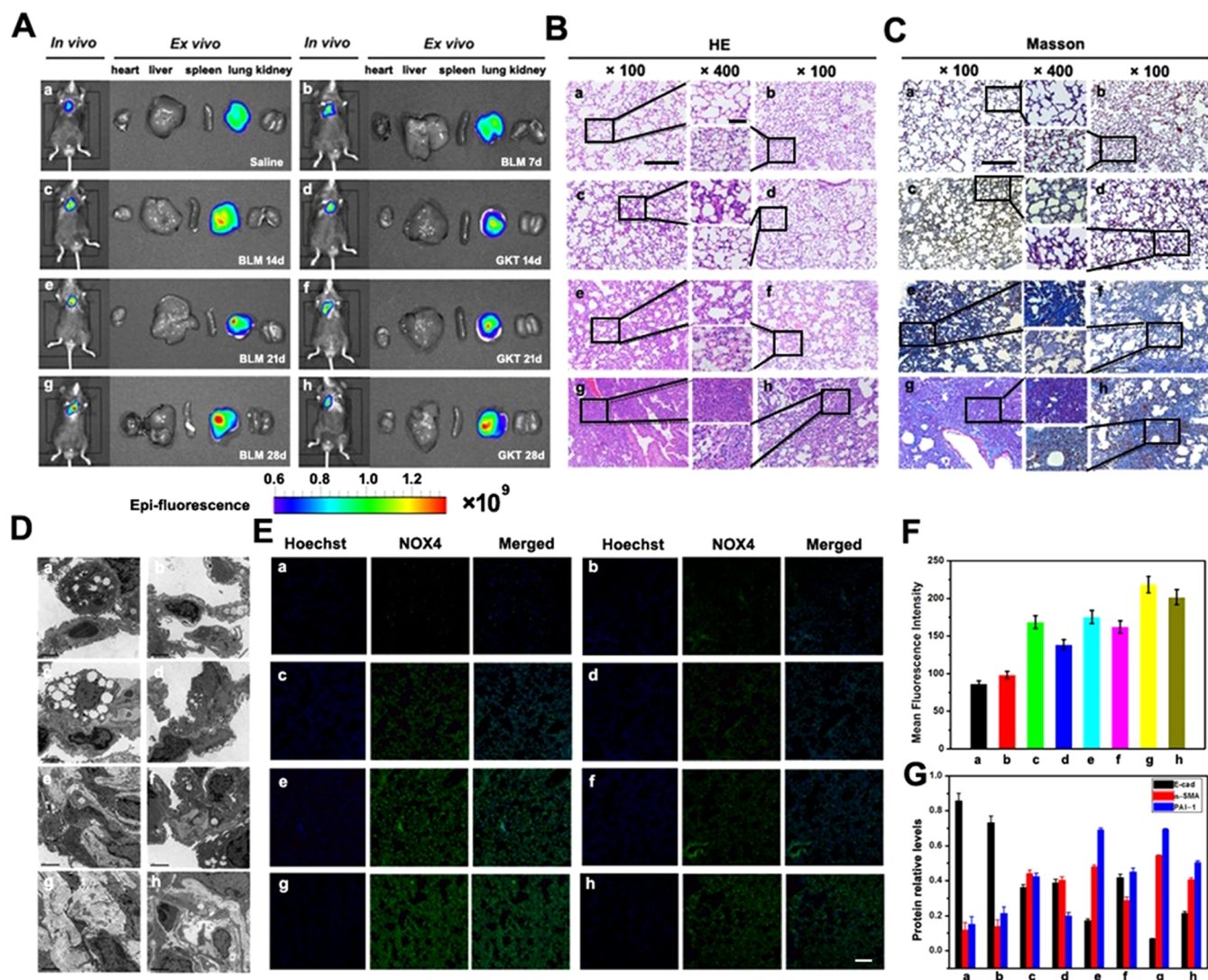


Figure 6. Fluorescence imaging of H_2O_2 level in bleomycin-induced pulmonary fibrosis bleomycin (BLM) mice models. (A) *In vivo* imaging and imaging of isolated organs showing changes in the H_2O_2 levels in the mice model of pulmonary fibrosis. The models were treated with the Mito-Bor probe ($10 \mu\text{M}$, $200 \mu\text{L}$, in DMSO/saline = 1:99, v/v) for 1 h via intratracheal spray. *In vivo* imaging reconstruction from the fluorescence collection window from 700 to 800 nm ($\lambda_{\text{ex}} = 710 \text{ nm}$). The mice in group a were injected with saline as the control group. Mice in group (b–h) received a single intratracheal instillation of bleomycin (5 mg/kg) for establishing pulmonary fibrosis models. After 7 days of intratracheal instillation of bleomycin, the mice in groups d, f, and h were treated with GKT137831 (60 mg/kg , twice a week) via gavage for 14, 21, and 28 days, respectively. In addition, the mice in group c, e, and g were treated with normal saline (twice a week) via gavage for 1, 2, and 3 weeks as control for group d, f, and h, respectively. (B) Hematoxylin–eosin staining (H&E) staining of the lung tissues in (A). (C) Masson staining of the lung tissues in (A). Scale bar: $100 \mu\text{m}$ in $100\times$ and $25 \mu\text{m}$ in $400\times$. (D) Transmission electron microscopy images of the lung tissues in (A). (E) Immunofluorescence imaging of NOX4 in mice lung tissues in (A). Scale bar: $20 \mu\text{m}$. (F) Fluorescence intensities of *in vivo* imaging in (A). (G) The relative protein analysis of E-cadherin, α -SMA, and PAI-1 in mice models of pulmonary fibrosis by ELISA.

differentiation, matrix synthesis, and contractility, as well as the mediation of a variety of profibrotic effects. This meant, NOX4 was not only one of the important sources of H_2O_2 in cells but also closely related to pulmonary fibrosis.^{53,54} Therefore, we employed immunofluorescence to assess the expression of NOX4 in IMR-90 cells and MRC-5 cells after the treatment of TGF- β 1. As illustrated in Figure 4D, blue fluorescence indicated nuclei that were stained with Hoechst 33342 and the bright green fluorescence revealed the high expression of NOX4 in the two types of cell lines. Compared with the control group, the prolongation of TGF- β 1 treatment resulted in changes in the cell morphology, including hypertrophied, elongated, and spindle-shaped (Figure S6). To assess changes in the intracellular level of H_2O_2 , IMR-90 cells and MRC-5

cells were pretreated with 5 nM TGF- β 1 for 24, 48, and 72 h, respectively. Then both cell lines were incubated with the Mito-Bor probe for 30 min at $37 \text{ }^\circ\text{C}$. The images in Figure 4E indicate that both cell groups provided stronger fluorescence intensity than those of control groups, demonstrating the increased level of H_2O_2 accompanied by the upregulation of NOX4. Flow cytometry analyses were well consistent with changes in fluorescent images (Figure 4F,G). The above results suggested that the level of H_2O_2 was positively correlated with the progress of TGF- β 1-induced fibrosis in the IMR-90 and MRC-5 cell models. Therefore, the abnormally high level of H_2O_2 might be utilized to indicate fibrosis degrees.

Effect of Endogenous H_2O_2 Levels on the Progression of Fibrosis. To explore the effect of endogenous H_2O_2 levels

during fibrosis progression, fibrotic IMR-90 cells and MRC-5 were cultured in serum-free medium. In the parallel groups, the two types of cells were stimulated with 5 nM TGF- β 1 for 72 h to induce the formation of fibrosis. Then the two cell lines were treated with a specific NOX4 inhibitor GKT137831 (GKT, 20 μ M) for 48 h to block fibrosis progression. Western blot analysis was utilized to examine the EMT of the IMR-90 and MRC-5 cells. As demonstrated in Figure 5A, the two cell lines, which were treated with TGF- β 1 displayed decreased expression of E-cadherin but increased expression of α -SMA. Compared to the control group, the levels of PAI-1 were also significantly upregulated. After inhibition of fibrosis progression by GKT, the cells showed a distinct trend of upregulation of E-cadherin and downregulation of α -SMA and PAI-1 (Figure 5B,C). The results suggested that the treatment with GKT could obstruct the EMT process as well as collagen deposition to a certain extent. Immunofluorescence analyses were employed to evaluate the activity of NOX4. As shown in Figure 5D, IMR-90 and MRC-5 cells in the control group emitted faint fluorescence, revealing a low level of NOX4. Upon treatment with TGF- β 1, strong green fluorescence indicated a high level of NOX4 than the cells in the control group. As expected, the two cell lines in the GKT treatment group exhibited weaker fluorescence than the TGF- β 1 treated cells. These results proved that the treatment with GKT might block fibrosis progression by inhibiting the activity level of NOX4. We next utilized the Mito-Bor probe to assess changes in the intracellular level of H₂O₂ in the IMR-90 and MRC-5 cells. Both cell lines were incubated with the Mito-Bor (10 μ M) for 30 min at 37 °C prior to the laser confocal imaging and flow cytometry analysis (Figure 5E–G). As shown in Figure 5E, the control group displayed faint fluorescence; however, the stimulation of TGF- β 1 resulted in strong red fluorescence emission, indicating high levels of intracellular H₂O₂. By suppressing NOX4 using GKT, the fluorescence intensities of the cells were decreased, implying low levels of H₂O₂ in these cell models. The results of flow cytometry analysis in Figure 5F,G showed a good correlation with the results of fluorescence imaging. These results demonstrated that the fibrosis progression would lead to increased H₂O₂ production. The disruption of fibrosis via GKT inhibition of NOX4 could decrease the H₂O₂ level. Therefore, the H₂O₂ level might directly reflect not only the fibrosis degree but also the therapeutic effects.

Examination of Changes in H₂O₂ Levels in Bleomycin-Induced Pulmonary Fibrosis Mice Models. Having detected changes in the level of H₂O₂ during fibrosis progression in cell models, we next applied the Mito-Bor probe for imaging changes in H₂O₂ levels in pulmonary fibrosis mice models. As illustrated in Figure 6, the mice in group a were injected with normal saline for 7 days as control. All other mice models of pulmonary fibrosis were established by a single intratracheal instillation of bleomycin to mice (5 mg/kg) for 7 days. Afterward, the mice in the testing groups d, f, and h were administrated with GKT137831 (60 mg/kg, twice a week), and those in control groups c, e, and g were treated with normal saline via gavage for 14, 21, and 28 days, respectively. As shown in Figure 6A,F, the Mito-Bor probe (10 μ M, 200 μ L, in DMSO: saline = 1:99, v/v) was employed for imaging H₂O₂. The mice models were treated with Mito-Bor for 1 h via intratracheal spray and then imaged via a small animal imaging system. The control group a emitted faint fluorescence, indicating the low physiological H₂O₂ concentration. The

fluorescence intensity of group b was stronger than that of group a, implying that the level of H₂O₂ in the lungs increased after 7 days of treatment with bleomycin. As expected, upon increasing the time of administration of GKT from day 14 to 21 and 28, the fluorescence intensity of the lungs in groups d, f, and h became stronger and stronger. The results demonstrated that with the degree of fibrosis, the level of H₂O₂ in the lungs increased. The corresponding GKT therapy groups d, f, and h exhibited lower fluorescence than the pulmonary fibrosis mice in groups c, e, and g, suggesting relatively low levels of H₂O₂. The results illustrated that the development of fibrosis contributed to high levels of H₂O₂, and the oxidative stress caused by H₂O₂ would promote the deterioration of the disease. The NOX4 inhibitor GKT could reduce the level of H₂O₂ to a certain extent, and therefore, delay the progress of pulmonary fibrosis. The positive correlation between the H₂O₂ level and fibrosis degree might be utilized to evaluate disease development and the curative effect. Moreover, the result suggested that during the treatment of pulmonary fibrosis, additional drugs should be supplemented to control the high level of H₂O₂ for reducing the damage caused by oxidative stress.

We also examined the pathological changes and related protein expression. Hematoxylin–eosin staining (H&E) and Masson staining were performed to determine changes in the lung alveoli and interstitium (Figure 6B,C). In the control group a, the alveolar wall remained complete. A small number of inflammatory cells infiltrated the alveolar wall due to the stimulation of normal saline, and no other fibrotic pathological changes were observed. For the bleomycin model groups, after the treatment for 7 days (group b), inflammatory cell infiltration and alveolar structure disorders were observed and worsened after 14 days (group c). Until 21 and 28 days (groups e and g), the alveolar wall became thick following the disappearance of normal alveolar structure, and the number of fibroblasts increased with collagen fiber deposition. In the late stage of fibrosis, the alveolar diaphragm was almost full of blue collagen fibers. Although histological biopsy of the GKT treatment groups (groups d, f and h) were similar to those of the model groups, at each time point, the typical inflammation infiltration and thickness of alveolar wall were alleviated than those of the bleomycin model groups, and the deposition of collagen fibers in the alveolar septum was relatively reduced. Transmission electron microscopy (TEM) was used to verify the histological changes in mice models (Figure 6D). Swollen type II epithelial cells were observed in the tissue of the 7-day mice model (group b). The mice in the 14-day group (c) showed swelling of type II epithelial cells, accompanied by the folding and thickening of the basement membrane. Additionally, microvilli passivation of type II epithelial cells increased and bundled collagen fibers appeared around alveolar epithelial cells. However, for the corresponding GKT-treated group d, only swelling of type I epithelial cells and much fewer collagen fibers distributed around the epithelial cells were observed. The 21-day and 28-day groups (e and g) displayed the accumulation of collagen fibers which would fill the intercellular spaces. Although the collagen fibers in the GKT-treated groups (f and h) gradually increased, the pathological changes were significantly less than those of the model groups (e and g). These results suggested that the intervention with GKT could weaken fiber accumulation and delay the progression of pulmonary fibrosis. Changes in the level of NOX4 in the mice lung tissues were also confirmed via

immunofluorescence assay (Figure 6E). The neglectable fluorescence in control group implied a low concentration of NOX4. However, stronger fluorescence was observed in group b, indicating higher levels of NOX4 after 7 days of treatment with bleomycin. The gradually increased fluorescence in group c, e, and g indicated the increased level of NOX4 with the increase of time. Upon treatment with GKT, the weaker fluorescence in group d, f, and h again proved the inhibition of NOX4 and decelerated fibrosis progression. Additionally, the fibrosis-relative protein was evaluated with ELISA. It was observed that the levels of E-cadherin decreased due to fibrosis progression, while the α -SMA and PAI-1 upregulated. However, the protein changes showed a reverse trend upon treatment with GKT. These indicated changes in the severity of fibrosis with treatment, which performed the same change behavior with the fluorescence changes (Figure 6F,G). In the bleomycin-induced pulmonary fibrosis mice model, GKT intervention could reduce the level of oxidative stress in the lungs and could delay the progression of the disease.

CONCLUSIONS

In summary, we have designed and synthesized a mitochondria-targeted near-infrared fluorescent probe Mito-Bor for detecting changes in the level of endogenous H_2O_2 in living cells and in pulmonary fibrosis mice models. The probe exhibits excellent photochemical stability, high sensitivity, and selectivity toward H_2O_2 . After confirming the capability of H_2O_2 detection in A549 and PC9 cells, the probe is used to sense fluctuations in the levels of endogenous H_2O_2 during the establishment of pulmonary fibrosis cell models. The results demonstrate that the level of intracellular H_2O_2 increases during the progression of fibrosis, while GKT137831, an inhibitor of NOX4, can downregulate the level of H_2O_2 and reduce intracellular oxidative stress, which may be utilized to weaken the pathological changes and delay the progression in fibrosis. Finally, the Mito-Bor probe is used to detect changes in the level of endogenous H_2O_2 in bleomycin-induced pulmonary fibrosis mice models. The experimental results including those of *in vivo* fluorescence imaging, histological tissue sections, transmission electron microscopy, and immunofluorescence, illustrate that changes in the level of H_2O_2 are closely related to the progression of pulmonary fibrosis. Taken together, we have confirmed the critical role of oxidative stress induced by H_2O_2 in the progression of pulmonary fibrosis. Our assay may shed light on the diagnosis and therapy of pulmonary fibrosis in the future.

ASSOCIATED CONTENT

Supporting Information

The Supporting Information is available free of charge at <https://pubs.acs.org/doi/10.1021/acssensors.0c02519>.

General experimental methods; additional materials and figures; synthesis steps; and compounds characterization (PDF)

AUTHOR INFORMATION

Corresponding Authors

Yanlong Xing – Key Laboratory of Emergency and Trauma, Ministry of Education, Key Laboratory of Hainan Trauma and Disaster Rescue, The First Affiliated Hospital of Hainan Medical University, Institute of Functional Materials and

Molecular Imaging, College of Pharmacy, College of Emergency and Trauma, Hainan Medical University, Haikou 571199, China; Email: xingyanlong@hainmc.edu.cn

Changjun Lv – Department of Respiratory Medicine, Binzhou Medical University Hospital, Binzhou 256603, China; Email: lucky_lcj@sina.com

Fabiao Yu – Key Laboratory of Emergency and Trauma, Ministry of Education, Key Laboratory of Hainan Trauma and Disaster Rescue, The First Affiliated Hospital of Hainan Medical University, Institute of Functional Materials and Molecular Imaging, College of Pharmacy, College of Emergency and Trauma, Hainan Medical University, Haikou 571199, China; orcid.org/0000-0003-0073-6299; Email: yufabiao@hainmc.edu.cn

Authors

Xinyu Song – Department of Respiratory Medicine, Binzhou Medical University Hospital, Binzhou 256603, China; Key Laboratory of Emergency and Trauma, Ministry of Education, Key Laboratory of Hainan Trauma and Disaster Rescue, The First Affiliated Hospital of Hainan Medical University, Institute of Functional Materials and Molecular Imaging, College of Pharmacy, College of Emergency and Trauma, Hainan Medical University, Haikou 571199, China; State Key Laboratory of Respiratory Disease, Guangzhou Institute of Respiratory Health, The First Affiliated Hospital of Guangzhou Medicine University, Guangzhou 510120, China

Song Bai – Department of Respiratory Medicine, Binzhou Medical University Hospital, Binzhou 256603, China

Na He – Department of Respiratory Medicine, Binzhou Medical University Hospital, Binzhou 256603, China

Rui Wang – Key Laboratory of Emergency and Trauma, Ministry of Education, Key Laboratory of Hainan Trauma and Disaster Rescue, The First Affiliated Hospital of Hainan Medical University, Institute of Functional Materials and Molecular Imaging, College of Pharmacy, College of Emergency and Trauma, Hainan Medical University, Haikou 571199, China

Complete contact information is available at: <https://pubs.acs.org/10.1021/acssensors.0c02519>

Author Contributions

[†]X.S. and S.B. contributed equally to this work.

Notes

The authors declare no competing financial interest.

ACKNOWLEDGMENTS

This work was supported by Hainan Provincial High-level Talent Project (Nos. 2019RC210 and 2019RC220), Hainan Key Research and Development Project (Grant. ZDYF2020133), National Natural Science Foundation of China (Nos. 21904030, 21864011, and 21775162), CAMS Innovation Fund for Medical Sciences (2019-I2M-5-023), Nanhai Young-Talent Program of Hainan (Grant. 20202018 and 20202007), and Hundred Talent Program of Hainan (2018).

REFERENCES

(1) Hutchinson, J.; Fogarty, A.; Hubbard, R.; McKeever, T. Global incidence and mortality of idiopathic pulmonary fibrosis: a systematic review. *Eur. Respir. J.* **2015**, *46*, 795–806.

- (2) King, T. E., Jr; Bradford, W. Z.; Castro-Bernardini, S.; Fagan, E. A.; Glaspole, L.; Glassberg, M. K.; Gorina, E.; Hopkins, P. M.; Kardatzke, D.; Lancaster, L. A phase 3 trial of pirfenidone in patients with idiopathic pulmonary fibrosis. *N. Engl. J. Med.* **2014**, *370*, 2083–2092.
- (3) He, N.; Bai, S.; Huang, Y.; Xing, Y.; Chen, L.; Yu, F.; Lv, C. Evaluation of glutathione S-transferase inhibition effects on idiopathic pulmonary fibrosis therapy with a near-infrared fluorescent probe in cell and mice models. *Anal. Chem.* **2019**, *91*, 5424–5432.
- (4) Zhang, H.; Liu, J.; Liu, C.; Yu, P.; Sun, M.; Yan, X.; Guo, J.-P.; Guo, W. Imaging lysosomal highly reactive oxygen species and lighting up cancer cells and tumors enabled by a Si-rhodamine-based near-infrared fluorescent probe. *Biomaterials* **2017**, *133*, 60–69.
- (5) Wu, L.; Sedgwick, A. C.; Sun, X.; Bull, S. D.; He, X.-P.; James, T. D. Reaction-based fluorescent probes for the detection and imaging of reactive oxygen, nitrogen, and sulfur species. *Acc. Chem. Res.* **2019**, *52*, 2582–2597.
- (6) Yang, G.; Liu, Z.; Zhang, R.; Tian, X.; Chen, J.; Han, G.; Liu, B.; Han, X.; Fu, Y.; Hu, Z. A Multi-responsive Fluorescent Probe Reveals Mitochondrial Nucleoprotein Dynamics with Reactive Oxygen Species Regulation through Super-resolution Imaging. *Angew. Chem., Int. Ed.* **2020**, *59*, 16154–16160.
- (7) Jiao, X.; Li, Y.; Niu, J.; Xie, X.; Wang, X.; Tang, B. Small-molecule fluorescent probes for imaging and detection of reactive oxygen, nitrogen, and sulfur species in biological systems. *Anal. Chem.* **2018**, *90*, 533–555.
- (8) Liu, H.-W.; Chen, L.; Xu, C.; Li, Z.; Zhang, H.; Zhang, X.-B.; Tan, W. Recent progresses in small-molecule enzymatic fluorescent probes for cancer imaging. *Chem. Soc. Rev.* **2018**, *47*, 7140–7180.
- (9) Chen, X.; Tian, X.; Shin, I.; Yoon, J. Fluorescent and luminescent probes for detection of reactive oxygen and nitrogen species. *Chem. Soc. Rev.* **2011**, *40*, 4783–4804.
- (10) Belousov, V. V.; Fradkov, A. F.; Lukyanov, K. A.; Staroverov, D. B.; Shakhbazov, K. S.; Tersikh, A. V.; Lukyanov, S. Genetically encoded fluorescent indicator for intracellular hydrogen peroxide. *Nat. Methods* **2006**, *3*, 281–286.
- (11) Wen, Y.; Huo, F.; Yin, C. Organelle targetable fluorescent probes for hydrogen peroxide. *Chin. Chem. Lett.* **2019**, *30*, 1834–1842.
- (12) Luo, X.; Wang, R.; Lv, C.; Chen, G.; You, J.; Yu, F. Detection of selenocysteine with a ratiometric near-infrared fluorescent probe in cells and in mice thyroid diseases model. *Anal. Chem.* **2019**, *92*, 1589–1597.
- (13) Chen, X.; Wang, F.; Hyun, J. Y.; Wei, T.; Qiang, J.; Ren, X.; Shin, I.; Yoon, J. Recent progress in the development of fluorescent, luminescent and colorimetric probes for detection of reactive oxygen and nitrogen species. *Chem. Soc. Rev.* **2016**, *45*, 2976–3016.
- (14) Zheng, D.; Yang, Y.; Zhu, H. Recent progress in the development of small-molecule fluorescent probes for the detection of hydrogen peroxide. *TrAC, Trends Anal. Chem.* **2019**, *118*, 625–651.
- (15) Liu, Y.; Niu, J.; Nie, J.; Meng, F.; Lin, W. A mitochondria-targetable fluorescent probe with a large Stokes shift for detecting hydrogen peroxide in aqueous solution and living cells. *New. J. Chem.* **2017**, *41*, 3320–3325.
- (16) Sun, W.; Li, M.; Fan, J.; Peng, X. Activity-based sensing and theranostic probes based on photoinduced electron transfer. *Acc. Chem. Res.* **2019**, *52*, 2818–2831.
- (17) Tian, M.; Ma, Y.; Lin, W. Fluorescent probes for the visualization of cell viability. *Acc. Chem. Res.* **2019**, *52*, 2147–2157.
- (18) Gao, M.; Yu, F.; Lv, C.; Choo, J.; Chen, L. Fluorescent chemical probes for accurate tumor diagnosis and targeting therapy. *Chem. Soc. Rev.* **2017**, *46*, 2237–2271.
- (19) Li, X.; Gao, X.; Shi, W.; Ma, H. Design strategies for water-soluble small molecular chromogenic and fluorogenic probes. *Chem. Rev.* **2014**, *114*, 590–659.
- (20) Verwilt, P.; Kim, H. S.; Kim, S.; Kang, C.; Kim, J. S. Shedding light on tau protein aggregation: the progress in developing highly selective fluorophores. *Chem. Soc. Rev.* **2018**, *47*, 2249–2265.
- (21) Song, X.; Han, X.; Yu, F.; Zhang, J.; Chen, L.; Lv, C. A reversible fluorescent probe based on C[double bond, length as m-dash]N isomerization for the selective detection of formaldehyde in living cells and in vivo. *Analyst* **2018**, *143*, 429–439.
- (22) Lippert, A. R.; Van de Bittner, G. C.; Chang, C. J. Boronate oxidation as a bioorthogonal reaction approach for studying the chemistry of hydrogen peroxide in living systems. *Acc. Chem. Res.* **2011**, *44*, 793–804.
- (23) Mao, W.; Zhu, M.; Yan, C.; Ma, Y.; Guo, Z.; Zhu, W. Rational Design of Ratiometric Near-Infrared Aza-BODIPY-Based Fluorescent Probe for in Vivo Imaging of Endogenous Hydrogen Peroxide. *ACS Appl. Bio Mater.* **2020**, *3*, 45–52.
- (24) Wang, K.; Ma, W.; Xu, Y.; Liu, X.; Chen, G.; Yu, M.; Pan, Q.; Huang, C.; Li, X.; Mu, Q.; Sun, Y.; Yu, Z. Design of a novel mitochondria targetable turn-on fluorescence probe for hydrogen peroxide and its two-photon bioimaging applications. *Chin. Chem. Lett.* **2020**, *31*, 3149–3152.
- (25) Xu, J.; Zhang, Y.; Yu, H.; Gao, X.; Shao, S. Mitochondria-targeted fluorescent probe for imaging hydrogen peroxide in living cells. *Anal. Chem.* **2016**, *88*, 1455–1461.
- (26) Chen, X.; Ren, X.; Zhang, L.; Liu, Z.; Hai, Z. Mitochondria-Targeted Fluorescent and Photoacoustic Imaging of Hydrogen Peroxide in Inflammation. *Anal. Chem.* **2020**, *92*, 14244–14250.
- (27) Wang, W.; Jiang, W.-L.; Liu, Y.; Li, Y.; Zhang, J.; Li, C.-Y. Near-infrared fluorescence probe with a large Stokes shift for visualizing hydrogen peroxide in ulcerative colitis mice. *Sens. Actuators, B* **2020**, *320*, No. 128296.
- (28) Gu, T.; Mo, S.; Mu, Y.; Huang, X.; Hu, L. Detection of endogenous hydrogen peroxide in living cells with para-nitrophenyl oxoacetyl rhodamine as turn-on mitochondria-targeted fluorescent probe. *Sens. Actuators, B* **2020**, *309*, No. 127731.
- (29) Jiang, W.-L.; Wang, W.-X.; Liu, J.; Li, Y.; Li, C.-Y. A novel hepatocyte-targeting ratiometric fluorescent probe for imaging hydrogen peroxide in zebrafish. *Sens. Actuators, B* **2020**, No. 128054.
- (30) Abo, M.; Urano, Y.; Hanaoka, K.; Terai, T.; Komatsu, T.; Nagano, T. Development of a highly sensitive fluorescence probe for hydrogen peroxide. *J. Am. Chem. Soc.* **2011**, *133*, 10629–10637.
- (31) Dong, B.; Song, X.; Kong, X.; Wang, C.; Tang, Y.; Liu, Y.; Lin, W. Simultaneous Near-Infrared and Two-Photon In Vivo Imaging of H₂O₂ Using a Ratiometric Fluorescent Probe based on the Unique Oxidative Rearrangement of Oxonium. *Adv. Mater.* **2016**, *28*, 8755–8759.
- (32) Reja, S. I.; Gupta, M.; Gupta, N.; Bhalla, V.; Ohri, P.; Kaur, G.; Kumar, M. A lysosome targetable fluorescent probe for endogenous imaging of hydrogen peroxide in living cells. *Chem. Commun.* **2017**, *53*, 3701–3704.
- (33) Yu, F.; Li, P.; Song, P.; Wang, B.; Zhao, J.; Han, K. Facilitative functionalization of cyanine dye by an on–off–on fluorescent switch for imaging of H₂O₂ oxidative stress and thiols reducing repair in cells and tissues. *Chem. Commun.* **2012**, *48*, 4980–4982.
- (34) Ye, S.; Hu, J. J.; Yang, D. Tandem Payne/Dakin reaction: a new strategy for hydrogen peroxide detection and molecular imaging. *Angew. Chem., Int. Ed.* **2018**, *57*, 10173–10177.
- (35) Ye, S.; Hananya, N.; Green, O.; Chen, H.; Zhao, A. Q.; Shen, J.; Shabat, D.; Yang, D. A Highly Selective and Sensitive Chemiluminescent Probe for Real-Time Monitoring of Hydrogen Peroxide in Cells and Animals. *Angew. Chem., Int. Ed.* **2020**, *59*, 14326–14330.
- (36) Maeda, H.; Fukuyasu, Y.; Yoshida, S.; Fukuda, M.; Saeki, K.; Matsuno, H.; Yamauchi, Y.; Yoshida, K.; Hirata, K.; Miyamoto, K. Fluorescent probes for hydrogen peroxide based on a non-oxidative mechanism. *Angew. Chem., Int. Ed.* **2004**, *43*, 2389–2391.
- (37) Guo, H.; Chen, G.; Gao, M.; Wang, R.; Liu, Y.; Yu, F. Imaging of endogenous hydrogen peroxide during the process of cell mitosis and mouse brain development with a near-infrared ratiometric fluorescent probe. *Anal. Chem.* **2018**, *91*, 1203–1210.
- (38) Lippert, A. R.; Gschneidner, T.; Chang, C. J. Lanthanide-based luminescent probes for selective time-gated detection of hydrogen peroxide in water and in living cells. *Chem. Commun.* **2010**, *46*, 7510–7512.

(39) Lou, Z.; Li, P.; Sun, X.; Yang, S.; Wang, B.; Han, K. A fluorescent probe for rapid detection of thiols and imaging of thiols reducing repair and H₂O₂ oxidative stress cycles in living cells. *Chem. Commun.* **2013**, *49*, 391–393.

(40) Onoda, M.; Tokuyama, H.; Uchiyama, S.; Mawatari, K.-i.; Santa, T.; Kaneko, K.; Imai, K.; Nakagomi, K. Fluorescence enhancement by hydroperoxides based on a change in the intramolecular charge transfer character of benzofurazan. *Chem. Commun.* **2005**, 1848–1850.

(41) Cheng, P.; Zhang, J.; Huang, J.; Miao, Q.; Xu, C.; Pu, K. Near-infrared fluorescence probes to detect reactive oxygen species for keloid diagnosis. *Chem. Sci.* **2018**, *9*, 6340–6347.

(42) Guo, Z.; Park, S.; Yoon, J.; Shin, I. Recent progress in the development of near-infrared fluorescent probes for bioimaging applications. *Chem. Soc. Rev.* **2014**, *43*, 16–29.

(43) Song, X.; Han, X.; Yu, F.; Zhang, X.; Chen, L.; Lv, C. Polyamine-targeting gefitinib prodrug and its near-infrared fluorescent theranostic derivative for monitoring drug delivery and lung cancer therapy. *Theranostics* **2018**, *8*, 2217–2228.

(44) Huang, J.; Li, J.; Lyu, Y.; Miao, Q.; Pu, K. Molecular optical imaging probes for early diagnosis of drug-induced acute kidney injury. *Nat. Mater.* **2019**, *18*, 1133–1143.

(45) Cheng, P.; Miao, Q.; Li, J.; Huang, J.; Xie, C.; Pu, K. Unimolecular chemo-fluoro-luminescent reporter for crosstalk-free duplex imaging of hepatotoxicity. *J. Am. Chem. Soc.* **2019**, *141*, 10581–10584.

(46) Huang, J.; Lyu, Y.; Li, J.; Cheng, P.; Jiang, Y.; Pu, K. A Renal-Clearable Duplex Optical Reporter for Real-time Imaging of Contrast-induced Acute Kidney Injury. *Angew. Chem. Int. Ed.* **2019**, *58*, 17796–17804.

(47) Yang, Z.; Cao, J.; He, Y.; Yang, J. H.; Kim, T.; Peng, X.; Kim, J. S. Macro-/micro-environment-sensitive chemosensing and biological imaging. *Chem. Soc. Rev.* **2014**, *43*, 4563–4601.

(48) Shi, Z.; Han, X.; Hu, W.; Bai, H.; Peng, B.; Ji, L.; Fan, Q.; Li, L.; Huang, W. Bioapplications of small molecule Aza-BODIPY: from rational structural design to in vivo investigations. *Chem. Soc. Rev.* **2020**, *49*, 7533–7567.

(49) Pacher, P.; Beckman, J. S.; Liaudet, L. Nitric oxide and peroxynitrite in health and disease. *Physiol. Rev.* **2007**, *87*, 315–424.

(50) Kliment, C. R.; Oury, T. D. Oxidative stress, extracellular matrix targets, and idiopathic pulmonary fibrosis. *Free Radicals Biol. Med.* **2010**, *49*, 707–717.

(51) Mora, A. L.; Bueno, M.; Rojas, M. Mitochondria in the spotlight of aging and idiopathic pulmonary fibrosis. *J. Clin. Invest.* **2017**, *127*, 405–414.

(52) Kuwano, K.; Nakashima, N.; Inoshima, I.; Hagimoto, N.; Fujita, M.; Yoshimi, M.; Maeyama, T.; Hamada, N.; Watanabe, K.; Hara, N. Oxidative stress in lung epithelial cells from patients with idiopathic interstitial pneumonias. *Eur. Respir. J.* **2003**, *21*, 232–240.

(53) Hecker, L.; Logsdon, N. J.; Kurundkar, D.; Kurundkar, A.; Bernard, K.; Hock, T.; Meldrum, E.; Sanders, Y. Y.; Thannickal, V. J. Reversal of persistent fibrosis in aging by targeting Nox4-Nrf2 redox imbalance. *Sci. Transl. Med.* **2014**, *6*, No. 231ra47.

(54) Moran, N. p38 kinase inhibitor approved for idiopathic pulmonary fibrosis. *Nat. Biotechnol.* **2011**, *29*, 301.